JOURNAL OF MATERIALS SCIENCE 20 (1985) 2148–2158

Production and properties of rapidly solidified Al–4.5% Cu alloy powder by the rotating-water-atomization process

ITSUO OHNAKA, ISAMU YAMAUCHI, SATORU KAWAMOTO, TATSUICHI FUKUSAKO
Department of Metallurgical Engineering, Osaka University, Suita-shi, Osaka, 565, Japan

Rapidly solidified Al–4.5 wt % Cu powder was produced by the rotating-water-atomization process recently developed by the authors. The particles were not spherical but tear-drop shape. The mean particle size of the powder decreased with increasing rotational speed of the drum and with decreasing nozzle diameter. The dendrite arm spacing of the particles produced was in the range 0.6 to 2.8 μm. The cooling rate was estimated to range from 10^3 to 5×10^5 K sec^{-1}. Recrystallization of hot extruded powder material after T6 treatment was remarkably suppressed in the central part, while large fully recrystallized grains were obtained in the cast material extruded under the same conditions. Tensile strength of the powdered material extruded in the range 573 to 723 K was slightly higher than the extruded cast material with little loss in elongation. The surface oxidation was not deleterious to elongation but it was very effective in suppressing recrystallization.

1. Introduction

New materials with improved mechanical or physical properties can be developed by the rapid solidification process associated with reduction of segregation, refinement of secondary phases and suppression or elimination of coarse primary phases [1].

In DC processing of commercial aluminium material, the mean cooling rate during solidification is estimated to be about 0.5 to 13 K sec^{-1} [2]. Therefore, coarse primary or secondary phases which are harmful to tensile strength sometimes appear in a DC ingot. Grant *et al.* [3], first reported that mechanical properties were much improved in a splat-cooled 2024 aluminium alloy. Recently, various kinds of rapid solidification processes have been applied to many aluminium alloys by combination with metal powder technology [4–12].

Characteristics such as cooling rate, shape and size distribution of the rapidly solidified particles or ribbons vary with the applied process. Properties of the final product strongly depend on these characteristics. Therefore, it is important for the evaluation of the process to describe these properties with reference to the applied process.

In this paper, the rotating-water-atomization (RWA) process, recently developed by the authors, was applied to produce rapidly solidified Al–4.5% Cu powder and the effect of process parameters such as nozzle diameter or water surface velocity on the particle size distribution was examined. The cooling rate of the particles produced was estimated from the dendrite arm spacing. Hot extrusion of the powder was attempted and then tensile tests were carried out.

The Al–4.5% Cu alloy is suitable to estimate the cooling rate because many researchers have previously reported the relation between the cooling rate and the dendrite arm spacing [13, 14].

2. Experimental procedure

2.1. Atomization

The RWA process was originally developed by the authors [15] as a modification of the in-rotating-water-spinning process (IRWSP) [16, 17]. A

0022–2461/85 $03.00 + .12

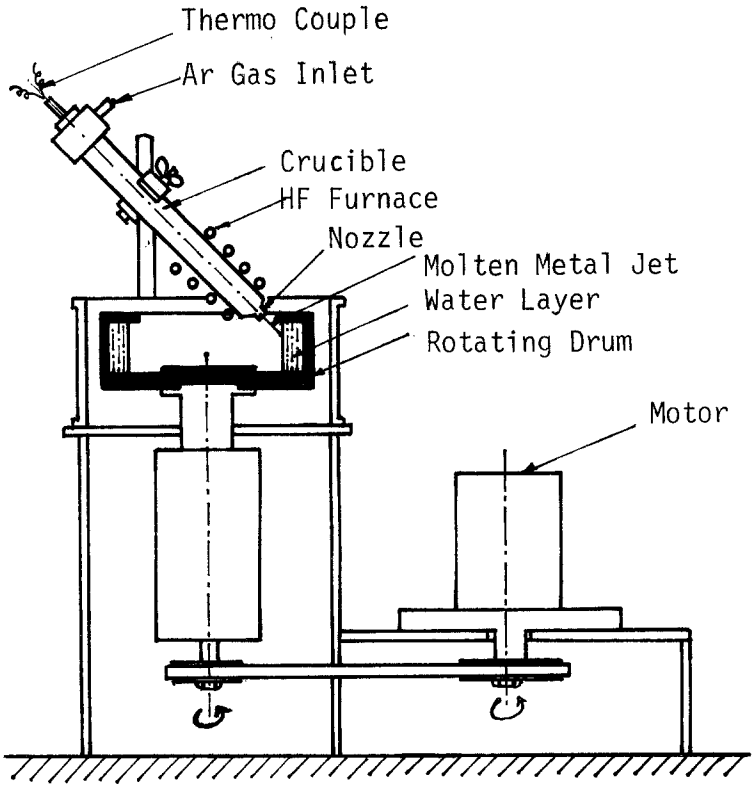

Figure 1 Laboratory scale rotating-water-atomization unit.

similar process also independently has been developed at Battelle's Columbus Laboratory [18].

The laboratory scale RWA unit is shown in Fig. 1. In this process, the molten metal jet ejected through the nozzle was atomized and rapidly cooled by the rotating water layer formed on the inner surface of the rotating drum by the centrifugal force.

In some atomization experiments, a quartz tube was used as a nozzle so that the diameter of the nozzle can be easily changed from 0.21 to 1.0 mm. The influence of the nozzle diameter on the mean particle size was examined by using this quartz nozzle. The graphite nozzle with 0.5 mm diameter was used to produce powder for hot extrusion. In the case of the quartz tube, 0.1% Be was added to the Al–4.5% Cu alloy to avoid the reaction between the quartz and the molten metal. The molten metal jet was ejected onto the rotating water layer by argon gas at 0.05 to 0.2 MPa pressure. The rotational speed of the rotating water layer was in the range of 8.4 to 76 m sec^{-1}. The ejection temperature was 1023 K. The charge for each run was about 10 to 20 g.

After the atomization, the atomized powder was cleaned using methanol and rapidly dried in a vacuum. The size distribution was measured by sieving. The shape of obtained particles was observed by scanning electron microscopy (SEM). The microstructure observations were carried out on beryllium free Al–4.5% Cu alloy particles.

2.2. Hot extrusion

The flow of the hot extrusion process is shown in Fig. 2. Particles passed through a 48 mesh sieve (i.e. smaller than about 300 μm) were used for hot extrusion. These particles were well mixed. About 5 g of them were compacted at room temperature into a cylindrical shape of 9.8 mm in diameter and 30 mm in height at a pressure of 325 MPa for about 20 sec.

The apparent porosity at 325 MPa compaction was about 12%. The compacted sample had enough strength to handle and it was degassed in a vacuum of 0.13×10^{-2} Pa at the same temperature as the hot extrusion for 1 h and then air cooled. If this vacuum degassing process was omitted, some blisters were often observed in the hot extruded material.

The hot extrusion was carried out at the rate of 0.06 to 0.08 mm sec^{-1} and the extrusion ratios used were 4 or 11. To compare mechanical properties of the hot extruded powder material with

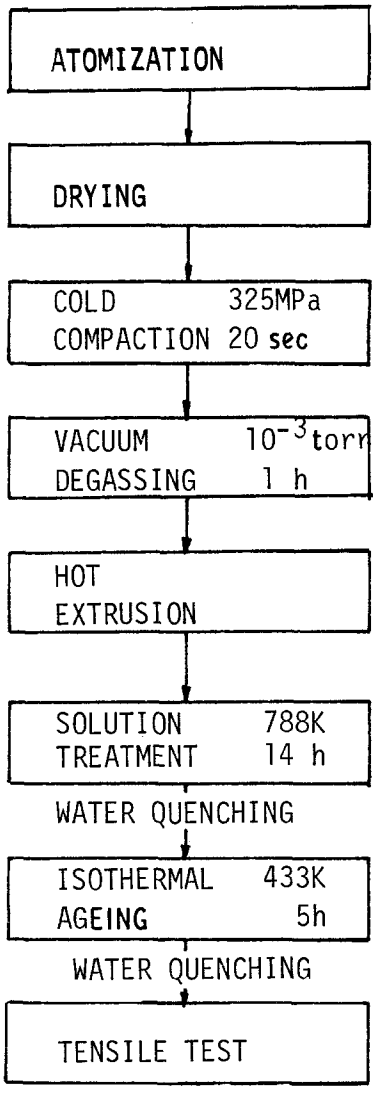

Figure 2 Flow of hot extrusion process.

conventional cast material an Al–4.5% Cu alloy was also cast into a graphite mould of 9.8 mm inner diameter and then extruded under the same condition. After the extrusion solution treatment was carried out at 788 K for 14 h and then isothermal ageing was conducted at 433 K for 5 h (T6 treatment). The tensile test was carried out at a strain rate of 8.3×10^{-3} using an Instron-type machine.

3. Experimental results and discussion

3.1. Shape of particles

The particle shape was not spherical but tear-drop as shown in Fig. 3. It is said that the conventional gas atomization of aluminium produces spherical and tear-drop particles under inert and oxidizing atmospheres, respectively. It is suggested that

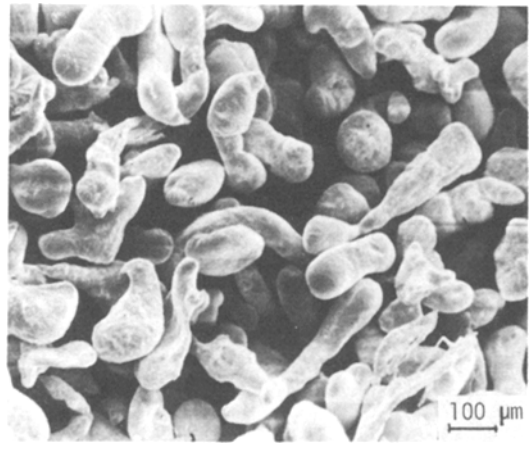

Figure 3 SEM micrograph of powders. ($D_n = 0.5$ mm, $V_w = 41.9\ m\ sec^{-1}$).

some amount of oxide film layer may exist on the surface of each particle. The influence of such an oxide film on tensile properties will be discussed later in this paper (Section 3.4.2).

3.2. Size distribution

3.2.1. Effect of the nozzle diameter on the size distribution

Fig. 4 shows the variation of particle size distribution with the nozzle diameter including the result for an $Fe_{40}Ni_{40}B_{20}$ alloy [15]. The size distribution of the Al–4.5% Cu alloy moves to a coarser size than the $Fe_{40}Ni_{40}B_{20}$ alloy. The relation between the mean particle size $D_p(\mu m)$ defined as the diameter at 50% cumulative wt% and the cross sectional area of the nozzle $S_n(mm^2)$ was derived for a water surface velocity V_w of $41.9\ m\ sec^{-1}$ as:

$$D_p = 363\, S_n^{0.27} \quad (1)$$

3.2.2. Effect of rotating water surface velocity (V_w) on the size distribution

Fig. 5 shows the relation between the rotating water surface velocity and the size distribution. At low velocity the size of most particles was larger than the diameter of the nozzle used. At higher velocities finer particles were obtained. The mean particle size $D_p(\mu m)$ can be expressed by the following equation as a function of the water surface velocity $V_w(m\ sec^{-1})$ for a nozzle diameter D_n of 0.5 mm:

$$D_p = 17 \times 10^3\, V_w^{-1.2} \quad (2)$$

This expression shows that size distribution is

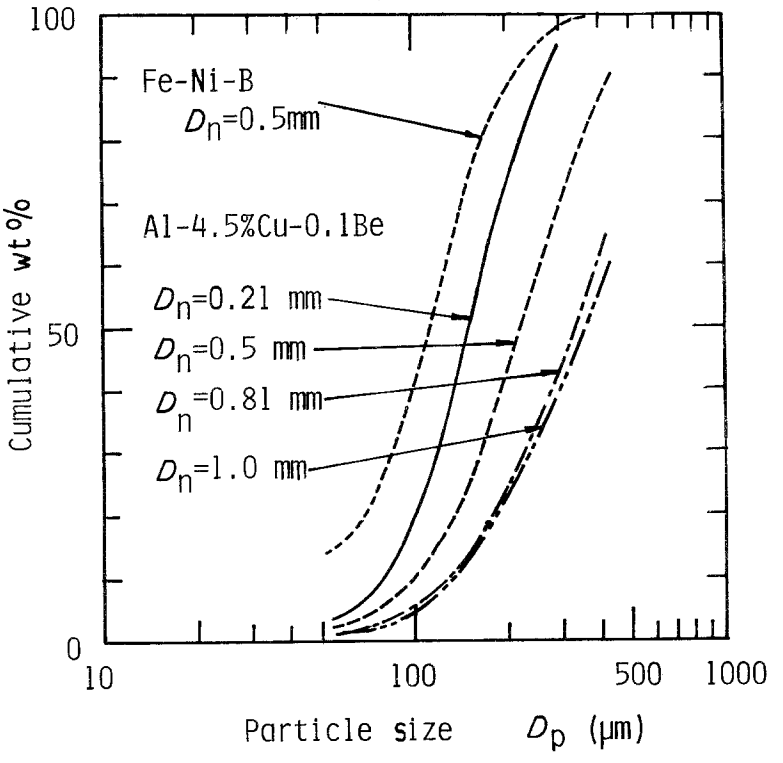

Figure 4 Effect of nozzle diameter on particle size distribution ($V_w = 41.9\,m\,sec^{-1}$).

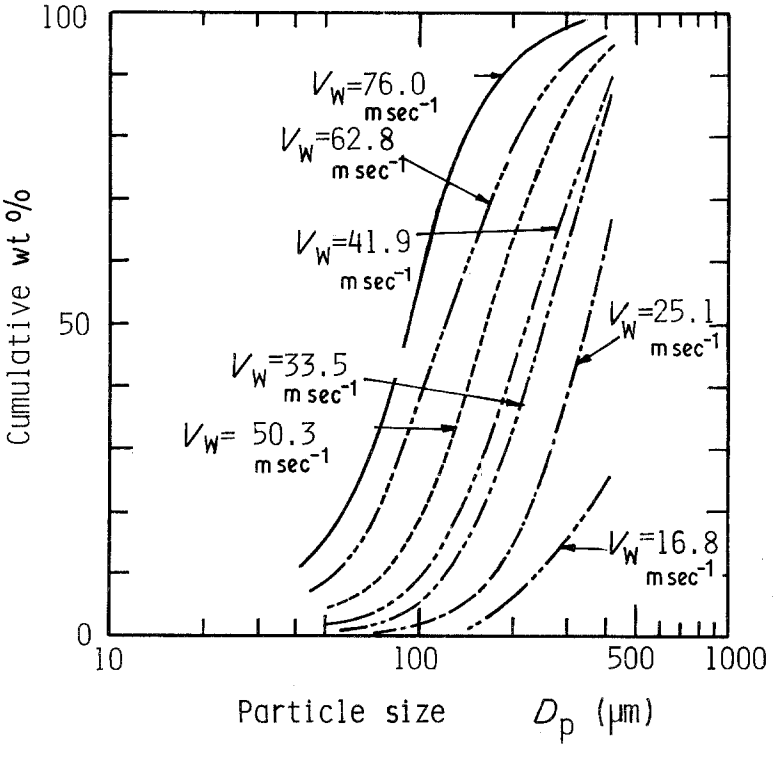

Figure 5 Effect of rotating water surface velocity on particle size distribution ($D_n = 0.5$ mm).

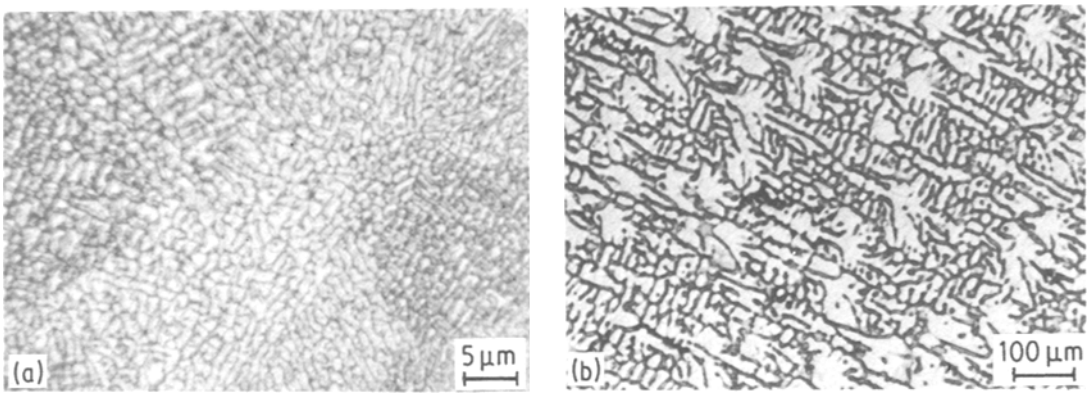

Figure 6 Microstructure of the Al–4.5% Cu alloy (a) as-atomized particle, (b) as-cast material into graphite mould.

strongly dependent on the velocity. In this experiment the applied maximum velocity was 76.0 m sec^{-1}. Even at the maximum velocity the mean diameter was not saturated but it seemed to be decreasing. It suggests that it is possible to get still finer particles by increasing the velocity. The power factor in Equation 2 was almost the same value for the $Fe_{40}Ni_{40}B_{20}$ alloy [15]. It may be suggested that the effect of the velocity on the mean particle size is almost independent of the alloy type.

3.3. Microstructure and cooling rate

A few particles larger than 420 μm in diameter sometimes showed an inhomogeneous structure with coarse or fine dendrite arm spacing varying in the location of the particle. In most of the particles under 420 μm, however, a fine homogeneous dendritic structure was observed as shown in Fig. 6a. This fact shows that the whole particle was cooled at almost the same rate and it follows that Newtonian cooling was dominant in this process.

The dendrite arm spacing varied from 0.6 to 2.8 μm from particle to particle. In smaller particles, slightly finer dendrites were observed. However, the relation between the particle size and the dendrite arm spacing was not clear. For comparison, the microstructure of as-cast material is shown in Fig. 6b. From the relation between the dendrite arm spacing and the cooling rate summarized by Mehrabian [13] and Matyja [14], the cooling rate was estimated to be in the range of 10^3 to 5×10^5 K sec^{-1}. In the RSR process which was developed by Pratt and Whitney [20] to produce rapidly solidified powder using helium gas, it was reported that the cooling rate increased with decreasing particle diameter as predicted by solidification analysis assuming Newtonian cooling. At the present time, it is not clear how this difference between the RWA and RSR processes has arisen. One possibility is that some of the particles were scattered on the water surface and not directly cooled by water. A part of this phenomenon was observed in stroboscopic photographs by the authors [15, 19]. Another possibility is that cooling conditions differ from particle to particle depending on the degree of boiling at the interface.

3.4. Hot extrusion

3.4.1. Structure of hot extruded material

A typical microstructure of the powdered material (PM) and cast material (CM) in the hot extruded condition is shown in Fig. 7. Elongated fibrous structures were observed along the extruded direction in both materials being coarser in CM. The recrystallized structure after T6 treatment is shown in Fig. 8a–d.

In CM, coarse and equiaxially recrystallized grains can be observed. On the other hand, in PM, the grain growth during the recrystallization was remarkably suppressed and the elongated recrystallized structure was obtained. A similar structure was observed in recrystallized sintered aluminium powder (SAP) material [21]. The finely dispersed oxide in the hot extruded material may be effective as a Zener drag barrier in the recrystallization process [22]. This fine recrystallized structure was obtained with a short heating time of 0.5 h at 788 K and hereafter the growth became negligibly slow.

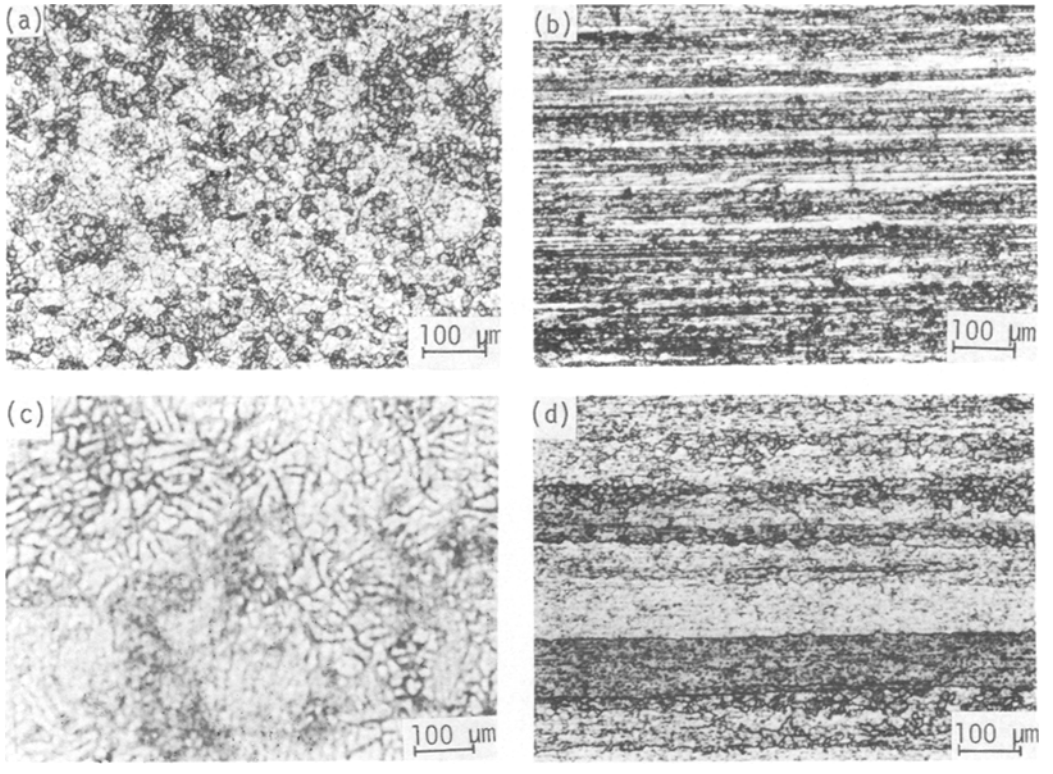

Figure 7 Structure of as-hot extruded PM and CM extruded at 673 K. (a) Cross-section of PM, (b) longitudinal section of PM, (c) cross-section of CM, (d) longitudinal section of CM.

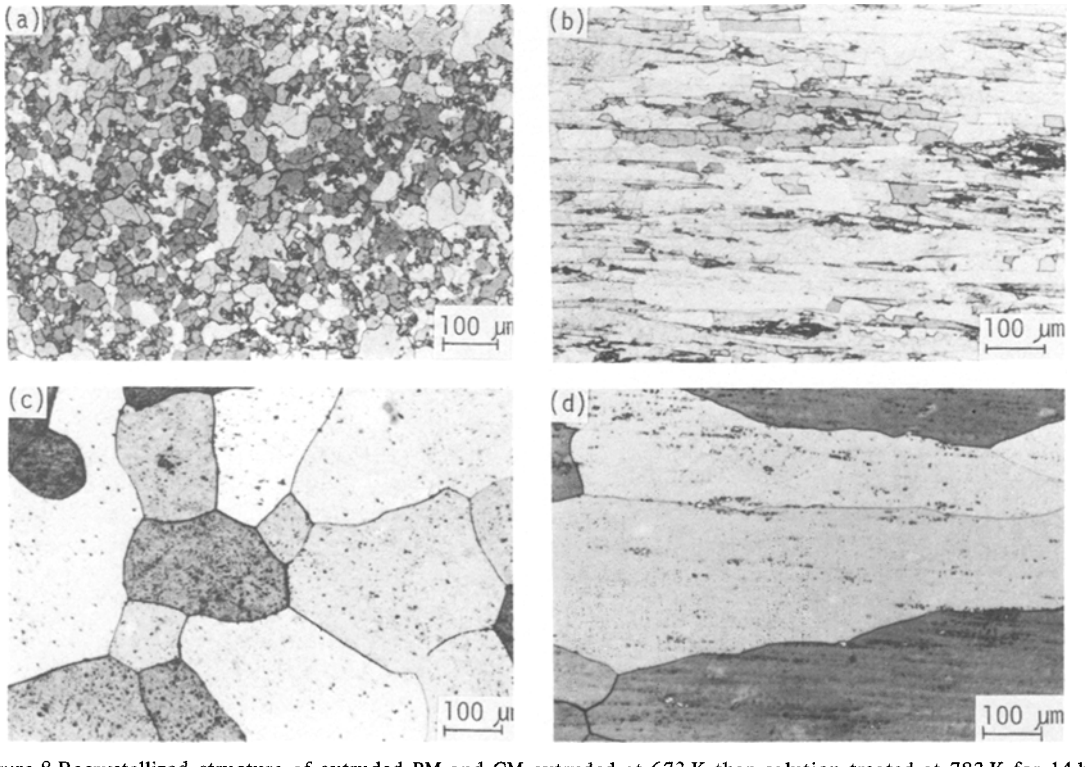

Figure 8 Recrystallized structure of extruded PM and CM extruded at 673 K then solution treated at 783 K for 14 h. (a) Cross-section of PM, (b) longitudinal section of PM, (c) cross-section of CM, (d) longitudinal section of CM.

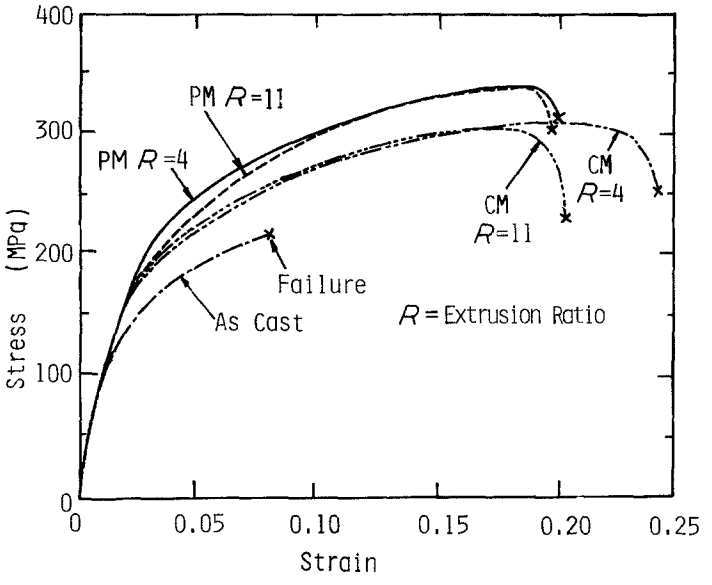

Figure 9 Stress–strain curve for PM and CM extruded at 673 K. (All samples were heat treated at 788 K for 14 h followed by ageing at 433 K for 5 h.)

3.4.2. Tensile properties

Some examples of the stress–strain curves for various PM and CM extruded at 673 K and an example of conventionally cast material are also shown in Fig. 9. The strength and elongation of the conventional cast material are the lowest values and may be caused by defects such as shrinkage porosity which had been observed on the fracture surface by SEM.

PM shows slightly lower elongation and higher tensile strength than CM. The oxide film may exist on the particle.

The oxygen analysis in aluminium alloys is not easy and it may be remarkably inaccurate depending on the kind of technique used. Nevertheless, about 150 to 300 ppm oxygen content was measured in the as-hot extruded PM by the carbon reduction method. This value is much smaller than conventional gas atomized powder [23], assuming this value is accurate. Quantitatively it should be examined in detail.

In order to roughly estimate the quantity of oxygen, 99.99% aluminium powder produced by the RWA process was extruded and the tensile properties were compared with SAP materials [24, 25]. The tensile strength of the 99.99% aluminium powder was about 57 MPa and the elongation was about 40%. These values suggests that oxygen content might be quite low at least less than 0.5%.

Loss of elongation due to the surface oxide film was negligible. It also had an advantage in suppressing grain growth during the T6 treatment and contributed to increasing the tensile strength.

For the Al–4.5% Cu alloy, the maximum solubility of Cu is 5.7% at 821 K, so all the θ phase in the inter-dendritic region is soluble during the solution treatment. Since T6 treatment is a usual heat treatment for this alloy, most of the advantages of the rapid solidification will be reduced during the solution treatment. However, as the dendrite arm spacing becomes finer due to the rapid solidification, the times for the solution treatment becomes shorter. Even after solution treatment (14 h at 788 K), a small amount of the θ phase still remained in the CM as small dark spots as shown in Fig. 8c and d, while such particles were hardly observed in PM as shown in Fig. 8a and b.

Fig. 10a shows the SEM fractograph of a fracture surface after tensile testing of the hot extruded CM. Fine slip lines can be seen at the arrow marked region in the relatively smooth surface domain of Fig. 10b which is a high magnification of A in Fig. 10a. It suggests that this type of the fracture may be caused by the "slipping-off" mechanism [26]. The size of the domain was almost equal to the grain size shown in Fig. 8c. It is likely that this slipping-off structure occurred at this particularly oriented grain.

The other parts of the failure specimen showed typical dimple patterns as shown in Fig. 10c and d, where small particles were seen in dimples. On the other hand, homogeneous failure patterns were obtained in PM material as shown in Fig. 11a–c. Domalavage *et al.* [27] observed delaminations on the tensile fracture surface along the extrusion axis

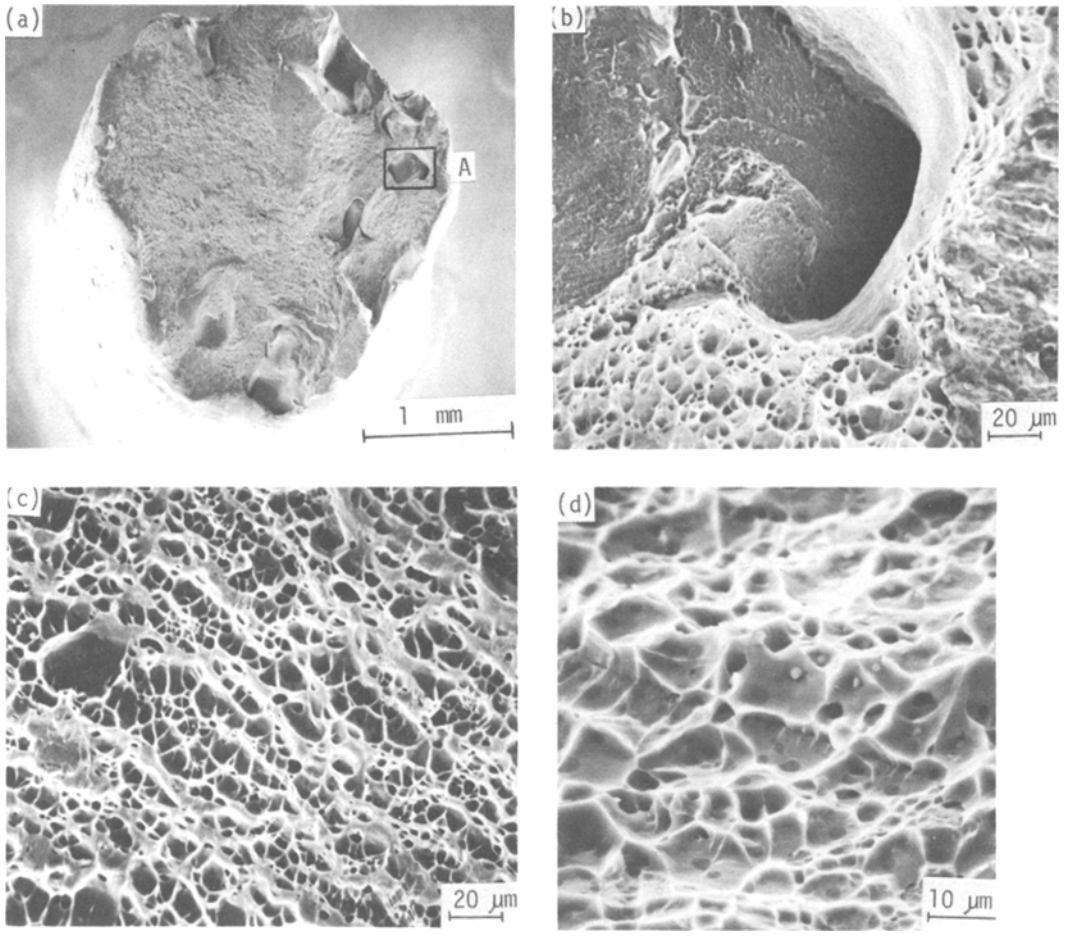

Figure 10 SEM micrographs of fracture surfaces of hot extruded Al–4.5% Cu CM extruded at 673 K. (a) Low magnification, (b) high magnification of region A in (a), (c) central region of (a), (d) high magnification of (b).

due to fine oxide particles axially arranged during the hot extrusion in 7075 alloy powder material prepared by an ultrasonic gas atomization process. The oxygen contents in their experiments were estimated to be 0.02 to 0.15 vol%. No delamination was observed in the Al–4.5% Cu alloy as shown in Fig. 11a but it appeared in an Al–Si alloy fabricated by the RWA process [28]. The influence of oxide on elongation may depend on the kind of alloy but it was negligible for the Al–4.5% Cu alloy. It is likely that most of the oxide changed from oxide film to finely dispersed particles during the hot extrusion.

3.4.3. Effect of extrusion temperature

Fig. 12 shows the variation of tensile strength and elongation with extrusion temperature. Even at the lowest temperature of 573 K in this experiment, the tensile strength and the elongation were almost the same as those at higher extrusion temperatures. This means that the extrusion temperature of 573 K is enough to get sufficient ductility. With increasing extrusion temperature, the extrusion load became slightly higher and a remarkably high tensile strength with negligible loss of elongation was obtained at 723 K. Its strength of 420 MPa is almost the same as that of Duralumin. Quite coarse recrystallized and fine grains were observed in the peripheral and central regions of extruded PM, respectively (Fig. 13a–d). On the other hand, in PM extruded at 783 K and T6 treated the grain size of the central region became slightly coarser than at lower extrusion temperatures and no coarse grains were observed in the peripheral region. The highest strength resulted from the finest grain sample.

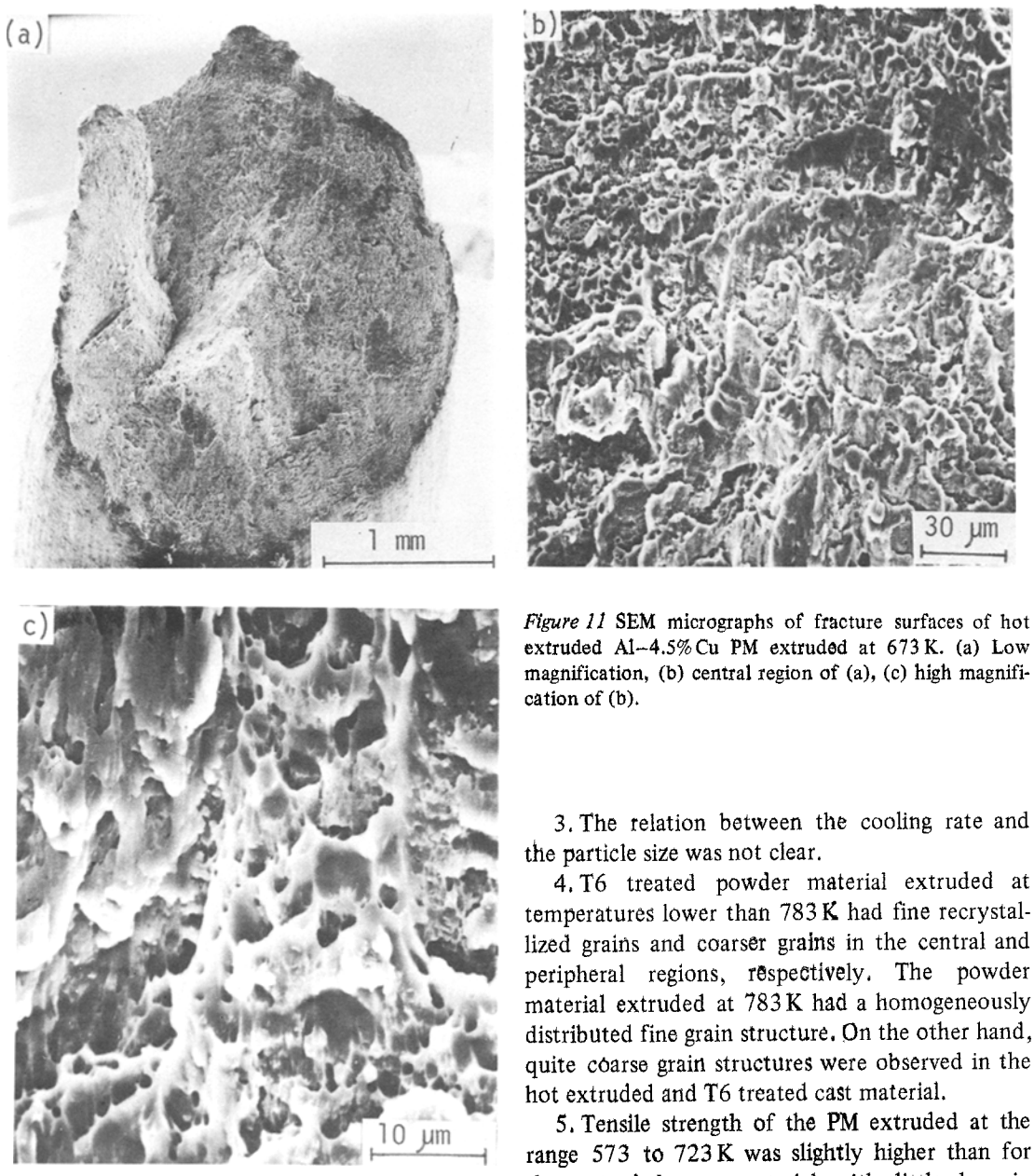

Figure 11 SEM micrographs of fracture surfaces of hot extruded Al–4.5% Cu PM extruded at 673 K. (a) Low magnification, (b) central region of (a), (c) high magnification of (b).

4. Conclusions

The RWA process has been applied to the Al–4.5% Cu alloy. Powder obtained has been hot extruded and tensile tests conducted. The results are as follows:

1. Tear-drop like particles were produced. The mean particle size decreased with increasing water surface velocity and decreasing nozzle diameter.

2. The dendrite arm spacing of the particles were from 0.5 to 3 μm and the cooling rate was estimated as 10^3 to 5×10^5 K sec^{-1}.

3. The relation between the cooling rate and the particle size was not clear.

4. T6 treated powder material extruded at temperatures lower than 783 K had fine recrystallized grains and coarser grains in the central and peripheral regions, respectively. The powder material extruded at 783 K had a homogeneously distributed fine grain structure. On the other hand, quite coarse grain structures were observed in the hot extruded and T6 treated cast material.

5. Tensile strength of the PM extruded at the range 573 to 723 K was slightly higher than for the extruded cast material with little loss in elongation. The oxide film on the particle surface was probably not deleterious to tensile strength and elongation and effectively suppressed the grain growth.

6. The highest tensile stress of the powdered material was obtained for a specimen extruded at 783 K. Its value of about 420 MPa was close to that of Duralumin.

Acknowledgements

The authors would like to thank Mr T. Ohmichi for his help with the experimental work.

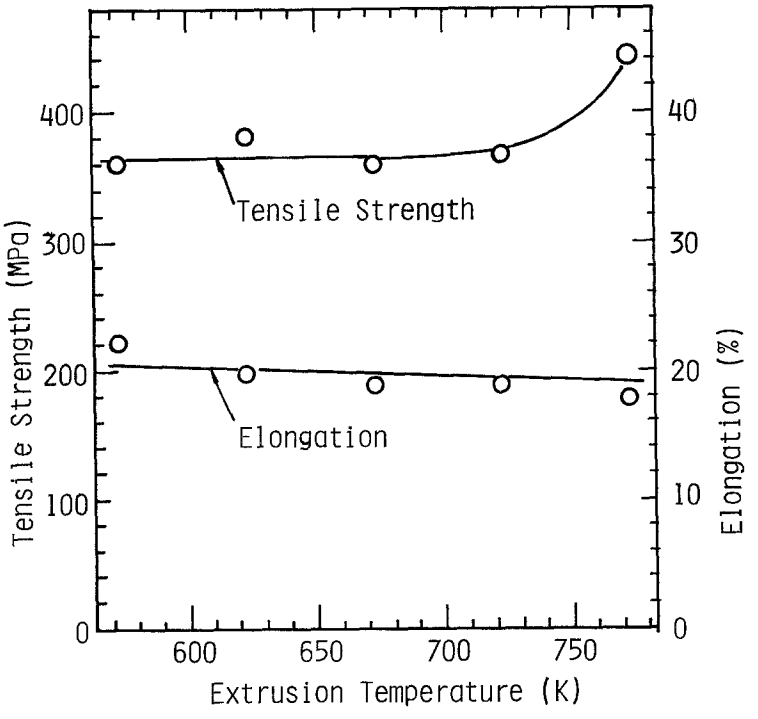

Figure 12 Variation of tensile properties with hot extrusion temperature.

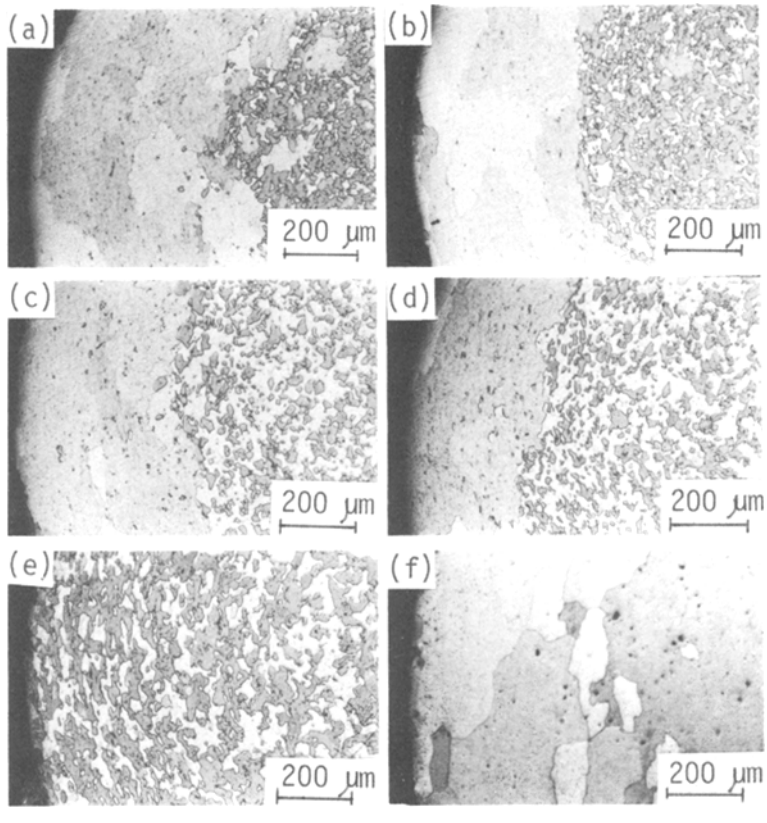

Figure 13 Effect of extrusion temperature on recrystallized structure in the peripheral region. (a) PM extruded at 573 K, (b) PM extruded at 633 K, (c) PM extruded at 673 K, (d) PM extruded at 733 K, (e) PM extruded at 783 K, (f) CM extruded at 783 K.

References

1. M. C. COHEN, B. H. KEAR and R. MEHRABIAN, "Rapid Solidification Processing, Principles and Technologies, II", edited by R. Mehrabian, B. H. Kear and M. C. Cohen (Claitor's Publishing Division, Louisiana, 1980) p. 1.
2. I. MIKI, H. KOSUGE and K. NAGAHAMA, *J. Jpn. Inst. Light Metals* **25** (1975) 1.
3. M. LEBO and N. J. GRANT, *Met. Trans.* **5** (1974) 1547.
4. G. THURSFIELD and M. J. STOWELL, *J. Mater. Sci. Eng.* **9** (1974) 1644.
5. J. P. MA. DURAND, R. M. PELLOUX and N. J. GRANT, *J. Mater. Sci. Eng.* **23** (1976) 247.
6. H. JONES, *Aluminium* **54** (1978) 274.
7. S. J. SAVAGE and H. JONES, Proceedings of the Fourth International Conference on Rapidly Quenched Metals, Sendai, 1981 (Japan Inst. Metals, 1982) p. 159.
8. J. R. PICKENS, *J. Mater. Sci.* **16** (1981) 1437.
9. R. YEARIM and D. SHECHTMAN, *Met. Trans.* **13A** (1982) 1891.
10. N. J. GRANT, *J. Metals* **35** (1983) 20.
11. T. SHEPPERED, M. A. ZAID and G. H. TAM, *Powder Met.* **26** (1983) 10.
12. P. K. DOMALVAGE, N. J. GRANT and Y. GEFEN, *Met. Trans.* **14A** (1983) 1599.
13. R. MEHRABIAN, "Rapid Solidification Processing and Technologies", edited by R. Mehrabian, B. H. Kear and M. C. Cohen (Claitor's Publishing Division, Lousiana, 1978) p. 9.
14. H. MATYJA, B. C. GIESSEN and N. J. GRANT, *J. Inst. Metals* **96** (1968) 30.
15. I. OHNAKA, T. FUKUSAKO and H. TSUTSUMI, *J. Jpn. Inst. Metals* **46** (1982) 1095.
16. I. OHNAKA, T. FUKUSAKO and T. OHMICHI, *ibid.* **45** (1981) 751.
17. T. MASUMOTO, I. OHNAKA, A. INOUE and M. HAGIWARA, *Scripta Metall.* **15** (1981) 293.
18. R. V. RAMAN, A. N. PATEL and R. S. CARBONARA, Proceedings of MPIF/AMPI, National Powder Metallurgy Conference (1982) Montreal, Canada.
19. I. YAMAUCHI, S. KAWAMOTO I. OHNAKA and F. FUKUSAKO, *J. Jpn. Inst. Metals* **47** (1983) 1016.
20. P. R. HOLLDAY, A. R. COX and R. J. PATTERSON II, "Rapid Solidification Processing and Technologies", edited by R. Mehrabian, B. H. Kear and M. C. Cohen (Claitor's Publishing Division, Louisiana, 1978) p. 246.
21. E. W. WESTERMAN and F. V. LENEL, *Trans. AIME* **218** (1960) 1010.
22. K. ITOH, *J. Jpn. Inst. Light Metals* **31** (1981) 497.
23. M. CHIBA and T. ANDO, *J. Jpn. Inst. Metals* **43** (1979) 1203.
24. R. IRMANN, *Metallurgia* **46** (1952) 125.
25. F. V. LENEL, A. B. BACKENSTO and M. V. ROSE, *Trans. AIME* **209** (1957) 124.
26. H. C. ROGERS, *ibid.* **218** (1966) 498.
27. P. K. DOMALAVAGE, N. J. GRANT and Y. GEFEN, *Met. Trans.* **14A** (1983) 1599.
28. I. YAMAUCHI, I. OHNAKA, S. KAWAMOTO and T. FUKUSAKO, to be published in *J. Jpn. Inst. Metals.*

Received 16 February
and accepted 31 July 1984